C. R. Mecanique 343 (2015) 133–142

Contents lists available at ScienceDirect

Comptes Rendus Mecanique

www.sciencedirect.com

Mechanics of granular and polycrystalline solids

Modeling the influence of particle morphology on the fracture behavior of silica sand using a 3D discrete element method

Mehmet B. Cil [1], Khalid A. Alshibli [*,2]

Dept. of Civil & Env. Engineering, University of Tennessee, 325 John Tickle Building, Knoxville, TN 37996, USA

ARTICLE INFO

Article history:
Received 13 February 2014
Accepted 26 August 2014
Available online 24 December 2014

Keywords:
Computed tomography
Fracture
Granular materials
DEM
Sand

ABSTRACT

The constitutive behavior and deformation characteristics of uncemented granular materials are to a large extent derived from the fabric or geometry of the particle structure and the interparticle friction resulting from normal forces acting on particles or groups of particles. Granular materials consist of discrete particles with a fabric (microstructure) that changes under loading. Synchrotron micro-computed tomography (SMT) has emerged as a powerful non-destructive 3D scanning technique to study geomaterials. In this paper, SMT was used to acquire in situ scans of the oedometry test of a column of three silica sand particles. The sand is known as ASTM 20–30 Ottawa sand, and has a grain size between US sieves #20 (0.841 mm) and #30 (0.595 mm). The characteristics and evolution of particle fracture in sand were examined using SMT images, and a 3D discrete element method (DEM) was used to model the fracture behavior of sand particles. It adopts the bonded particle model to generate a crushable agglomerate that consists of a large number of small spherical sub-particles. The agglomerate shape matches the 3D physical shape of the tested sand particles by mapping the particle morphology from the SMT images. The paper investigates and discusses the influence of agglomerate packing (i.e., the number and size distribution of spherical sub-particles that constitute the agglomerate) and agglomerate shape on the fracture behavior of crushable particles.

1. Introduction

Sand particle fracture has been extensively investigated by many researchers due to its profound influence on the behavior of sand. It has been examined at different scales, ranging from single particle level to laboratory specimen size. Researchers mainly adopted experimental, analytical, and numerical approaches to better understand and characterize the underlying micro-mechanics of particle fracture (e.g., [1–3]). Discrete Element Modeling (DEM) is a common discontinuum numerical method allowing one to model the breakage of particles in granular materials. The crushable nature of sand particles is generally represented using two common methods within the framework of DEM. The first method replaces a broken particle with a group of smaller particles based on a pre-defined failure criterion [4]. In the second method, researchers used an agglomerate composed of many bonded spherical sub-particles to represent the sand particles [5–8]. These studies provided a valuable contribution to the literature, allowing a better understanding of the fundamental behavior of crush-

* Corresponding author. Tel.: +11 865 974 7728.
E-mail addresses: mcil@utk.edu (M.B. Cil), Alshibli@utk.edu (K.A. Alshibli).
[1] Graduate student.
[2] Professor.

http://dx.doi.org/10.1016/j.crme.2014.11.004
1631-0721/

able particles, but none of the techniques already published could reproduce the 3D particle shape in DEM environment. Recently, Cil and Alshibli [9] proposed to use hexagonal and cubic packings of bonded spherical particles to generate an agglomerate in order to closely match the 3D physical shape of the particle. In this paper, the evolution of particle fracture and specimen deformation is investigated using a 3D DEM model with crushable agglomerates that match the 3D physical shape of silica sand particles via Synchrotron Micro-computed Tomography (SMT) images. This paper focuses on the improvement of the approach proposed by Cil and Alshibli [9] by adopting a different packing scheme, and investigates the characteristics of the particle fracture in granular materials by considering the variations in the distribution of spherical sub-particle sizes and in agglomerate packing.

2. Synchrotron Micro-computed Tomography (SMT) scans

SMT is a non-destructive in situ visualization technique that yields 3D high-resolution images of specimen by mapping X-ray attenuation data. SMT scans were acquired at GeoSoilEnviroCARS (GSECARS) Sector 13 of the Advanced Photon Source (APS), Argonne National Laboratory (ANL), Illinois, USA, a state-of-the-art synchrotron facility that provides a collimated and tunable high-energy X-ray beam. In a typical SMT setup, the specimen is positioned between the incoming X-ray source and detector system. As the X-rays travel through the specimen, some of the photons are absorbed by it, which depends on the chemical composition and the X-ray energy level. A scintillator is used to convert the transmitted X-rays to a visible light that is recorded using a CCD camera system. Each image provides attenuation data for a particular angle. A series of projection images needs to be acquired at different angles by rotating the specimen about an axis perpendicular to incident beam. The raw SMT data are processed to obtain the 3D spatial distribution map of the X-ray attenuation of the specimen, which is composed of stacks of 2D images.

In this study, SMT scans were acquired for a column composed of three sand particles that were subjected to 1D compression using beam-13D of APS. A special test cell that consists of a loading system, a specimen mold, load cells, and a data acquisition system was used in the experiments. The sand is ASTM 20-30 Ottawa sand; a natural silica sand with well-rounded particles that has a grain size between US sieves #20 (0.841 mm) and #30 (0.595 mm). To prepare a specimen, the sand particles were poured into a 1-mm cylindrical hole at the center of a 15-mm acrylic cylindrical mold and were compressed at a constant displacement rate of 0.2 mm/min. The SMT scans were acquired at an energy level of 23 keV that produced images with a spatial resolution of 4.95 μm/pixel. The sand column was scanned before applying the load; it was then loaded until the desired compressive load was reached, and another scan was performed while pausing loading. This procedure was repeated for consecutive load levels and scans. Fig. 1 shows an example load versus displacement relationship and axial cross sections of the 3D SMT images of the specimen at different displacement levels. Fig. 1a shows that the compressive load increases gradually as compression progresses. Some small load drops are observed due to particle movement and/or local asperity damage at particle contacts before the major fracture of one of the particles, which resulted in a significant drop in the load. Multiple small drops in load emerged after the initial fracture, which resulted from the continuous fracture of broken fragments of the fractured particle. The SMT images shown in Fig. 1b clearly illustrate the compressive behavior of sand particles under 1D compression. Initially, particles slightly rearrange through rotation and/or translation, and reach a stable configuration in which lateral support is provided by the mold walls. Then, the column of particles resists the increasing compressive load until fracture occurs in the form of catastrophic splitting. Both fractured and intact particles continue to fracture as the compression progresses.

3. DEM simulations

SMT images are 3D array structures that contain the spatial distribution map of the X-ray attenuation of the specimen. Raw scan data need to be analyzed to extract the 3D sand particle morphology. The first step in image analysis is to identify and separate each constituent material in the image, which was performed with the help of a segmentation process using Avizo Fire commercial software. Using the thresholding approach, SMT image was binarized by assigning a value of 1 for the sand particles and a value of 0 for the rest of the image, including the loading platens and acrylic cylindrical mold. Then, the 3D segmented binary image was saved as a text file to transfer particle shape information to PFC3D DEM software. The 3D view of the sand particles after segmentation is shown in Fig. 2b.

The 3D physical shapes of the silica sand particles were reproduced in DEM environment with the help of 3D SMT images. Initially, a prismoidal container was generated and filled with spherical particles that have a uniform grain size distribution defined by a minimum radius ($R_{\min}$) and a maximum radius ($R_{\max}$). The dimensions of the rectangular container were determined based on the dimensions of the 3D volume file of the SMT image (Fig. 2a). Then, the specimen was subjected to a relatively small isotropic compressive stress condition to obtain a densely packed specimen. After that, prismoidal DEM assembly and 3D segmented SMT image were compared in 3D space, and DEM particles that are corresponding to void space in segmented SMT image were deleted from the assembly (Fig. 2c). DEM particles corresponding to the volume occupied by silica sand particles in segmented SMT image were identified and categorized based on the corresponding sand particle. Then, the coordinates and radii of spherical sub-particles for each agglomerate were saved in a text file which is called an agglomerate template.

Sand particles were represented with agglomerates of bonded particles. Agglomerates were generated in a 1D compression test simulation using the position and size information of the spherical sub-particles in the agglomerate template files.

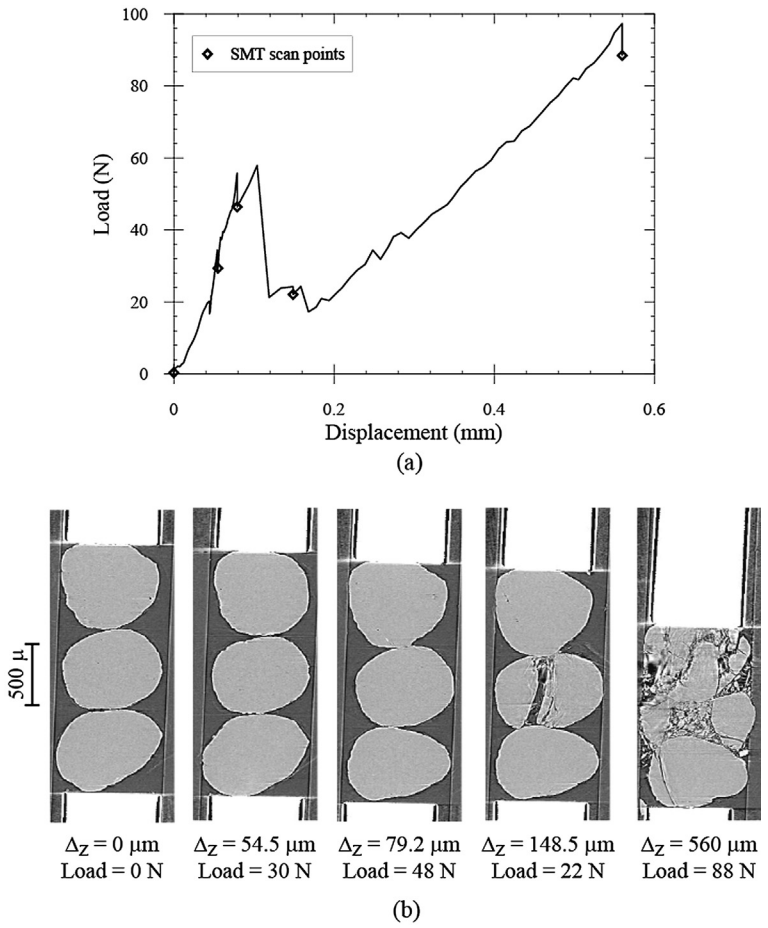

Fig. 1. (a) Load versus displacement relationship for 1D compression of a column of three sand particles; (b) axial cross-sectional images of the specimen acquired at different displacement levels. Reproduced with kind permission of Elsevier.

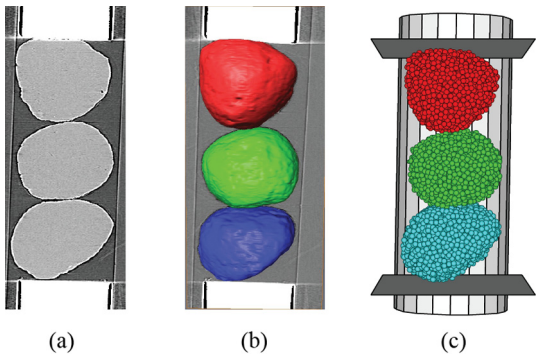

Fig. 2. (Color online.) (a) Axial cross section of the SMT image; (b) 3D rendering of the SMT image; and (c) DEM image of the column of three particles.

They have random packings of spherical sub-particles that closely match the 3D physical shape of the silica sand particles (Fig. 2c). Agglomerates have a void ratio of 0.54 that was adopted by Potyondy and Cundall [10] to obtain a densely packed assembly. A cylindrical wall and loading platens at the top and bottom of the specimen were generated in a DEM model based on the locations of end platens in SMT images. Then, DEM particle parameters were assigned to particles and parallel bonds were assigned to contact points. The specimen is allowed to reach a static equilibrium state by cycling under gravity forces. Finally, the specimen was subjected to compressional loading by moving the top loading platen downward at a constant displacement rate. The forces on loading platens, the evolution of particle fracture and the variation in contact force network were tracked throughout the simulations. DEM model parameters were inferred from Cil and Alshibli [9], and bond strength values were revised to capture the major particle fracture load level of the experiment by adopting an

Table 1
Summary of the PFC3D DEM model parameters.

Parameter	Value
Agglomerate:	
Density	2650 kg/m^3
Spherical sub-particles' properties:	
Minimum radius, R_{min}	0.021–0.033 mm
R_{max}/R_{min}	1.0–2.2
Friction coefficient	0.5
Normal and shear stiffness	8.0×10^6 N/m
Parallel bond:	
Bond radius multiplier	1.0
Normal stiffness	7.0×10^{14} N/m
Shear stiffness	3.0×10^{14} N/m
Normal and shear strength values	500 MPa

Table 2
Summary of the first set of DEM simulations.

Test	R_{min} (mm)	R_{max}/R_{min}	# of spherical sub-particles				Simulation time (min)
			Agg_1	Agg_2	Agg_3	Total	
Test_1a	3.30×10^{-2}	1.2	899	846	882	2627	24
Test_1b	2.90×10^{-2}	1.2	1324	1239	1305	3868	50
Test_1c	2.50×10^{-2}	1.2	2047	1946	2001	5994	102
Test_1d	2.10×10^{-2}	1.2	3438	3266	3388	10092	184

iterative calibration scheme. The same bond strength value was used in all three agglomerates. A summary of the DEM model parameters is listed in Table 1.

4. Results

During the calibration process of the DEM model, the simulation results demonstrated that many DEM parameters including the normal and shear stiffness values of the particles, the parallel bond properties, and the grain size distribution of the spherical sub-particles play a significant role in the overall response of the agglomerates. This paper focuses on investigating only the influence of agglomerate packing and size distribution of spherical sub-particles on the fracture behavior of agglomerates. The size distribution of spherical sub-particles defines the total number of particles within each agglomerate which influences the agglomerate overall shape. In order to investigate the effect of spherical sub-particle size, a series of simulations were performed by changing the size distribution of spherical sub-particles in two ways: shifting of the spherical size distribution, and varying the R_{min}/R_{max} ratio while keeping R_{min} constant.

4.1. Influence of sub-spherical particle size on the fracture behavior of the agglomerate

The R_{min} value is varied from 2.1×10^{-2} mm to 3.3×10^{-2} mm while keeping the value of R_{max}/R_{min} constant in order to examine its effect on deformation behavior and particle fracture. A summary of the DEM simulations is presented in Table 2. The specimen configurations before and after the DEM simulation are depicted in Fig. 3. In some cases, the load is directly transmitted to the main agglomerate structure through a group of particles that are in contact with the loading platen. In this case, some of the spherical sub-particles in the contact zone may have bond breakages and separate from the main agglomerate; however, the catastrophic major splitting fracture occurs when the agglomerate breaks into multiple fragments parallel to the maximum compressive force direction in the form of tensile failure. In some cases, the axial stress is localized at certain spherical sub-particles either at loading platen–agglomerate or agglomerate–agglomerate contact regions, which resulted in bond breakages in a group of spherical sub-particles at these contact interfaces. This type of local failure may be described as asperity damage seen in real sand particles. This fracture behavior leads to fluctuations in the load–displacement curve prior to a major tensile fracture of one of the agglomerates within the specimen.

Increasing the R_{min} value reduces the total number of spherical sub-particles in the model and decreases the execution time considerably. On the other hand, the shape of the sand particles can be mimicked more accurately with smaller R_{min} values. The profound influence of the variation of the value of R_{min} emerges on the load transmission behavior especially at the loading platen–agglomerate and agglomerate–agglomerate contacts. In order to identify this influence, the number and magnitude of contact forces were computed at the loading platen–agglomerate contacts (CP_1 and CP_4 in Fig. 4a) and agglomerate–agglomerate contacts (CP_2 and CP_3 in Fig. 4a) As an example, contact force analysis of Test_1a and Test_1d are presented in Fig. 4b–c, which demonstrates that there is a considerable variation in the number and magnitude of contact forces. The number of contacts is relatively small and contact forces are high at loading platen–agglomerate contacts (CP_1 and CP_4) compared to agglomerate–agglomerate contacts (CP_2 and CP_3). Moreover, the number of contacts de-

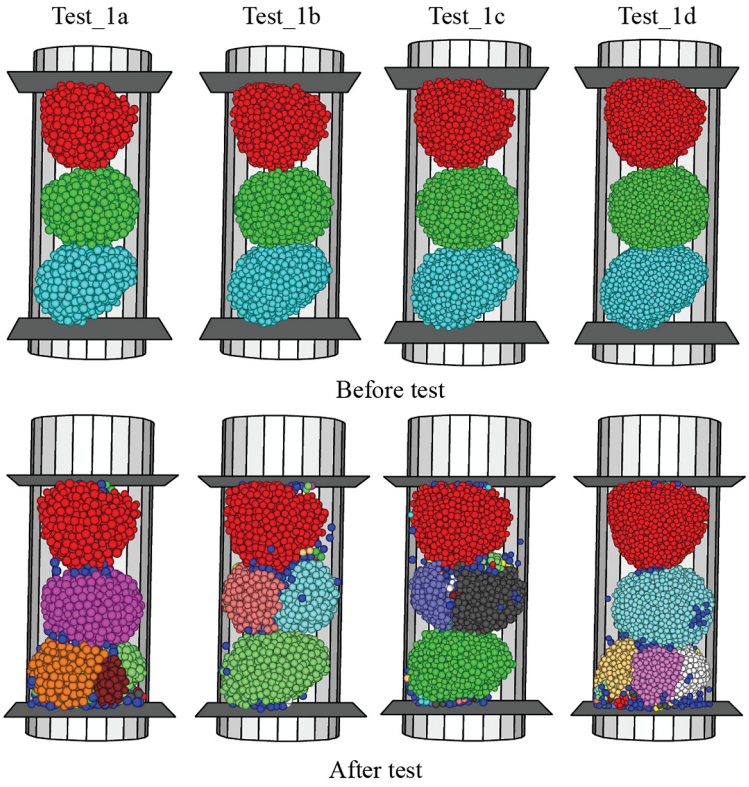

Fig. 3. (Color online.) Axial view of the first set simulations before and after 1D DEM compression simulations.

creases and the magnitude of contact forces increases as the value of R_{min} increases. These changes in contact force network seem relatively minor variations, but they lead to significant influence on initiation and growth of agglomerate fracture, as demonstrated in Fig. 3. A small number of contacts at CP_1 and CP_4 contacts resulted in force localization at certain points and fracture of the bonds. As the number of spherical sub-particles increases, the force is distributed to more particles and agglomerate becomes less vulnerable to localized failures.

The corresponding loads versus displacement relationships for the first set of DEM simulations are depicted in Fig. 5. All simulations exhibit nearly the same initial stiffness behavior at the initial stage of loading. Then, some agglomerates rotate and/or translate with increasing axial load and experience local asperity damage in the form of minor bond breakages at contact interfaces, as described earlier. These factors result in shifts in the load–displacement curve at ∼45–50 N range following the initial gradual increase. After these minor local failures, the load begins to increase continuously until experiencing a catastrophic tensile fracture in the form of major splits of the agglomerates. Then, the fluctuations are observed in the measured axial load until the end of the simulation. Many spherical sub-particles or particle groups that separate from the main agglomerate structure are displayed using different colors in Fig. 3 to demonstrate the evolution of fracture in each agglomerate.

In second set of DEM simulations, R_{min} value was kept constant at 2.5×10^{-2} mm, while varying the R_{max}/R_{min} ratio from 1.0 to 2.2 to investigate the size distribution effect in terms of the variation of sub-particle gradation. A summary of the DEM simulations is presented in Table 3 and the specimens before and after the DEM simulations are depicted in Fig. 6. Similar to the previous case, the distribution of spherical sub-particles significantly influences the force transmission mechanism in a column of three particles. As the R_{max}/R_{min} ratio increases from 1 to 2.2, the accuracy of the agglomerate in capturing the physical shape and surface of the silica sand particle decreases with the presence of coarse spherical sub-particles in the structure. The advantage of using a wide size distribution of spherical sub-particles is to better fill the voids between larger particles with smaller size ones, which provides a better agglomerate packing compared to the agglomerate generated using mono-sized spherical sub-particles. Moreover, the execution time decreases as the R_{max}/R_{min} value increase for a constant R_{min}.

Load versus displacement relationships for the second set of experiments are shown in Fig. 7. All DEM simulations produce almost the same initial elastic response, and relatively fewer local failures are observed in this set of simulations. The major particle failure in all simulations (except Test_2c) occurred almost at the same load level and then the load fluctuated until the end of the simulation after this failure point.

When compared to experimental results, DEM simulations exhibited many similarities as well as some differences. The 3D particle shape of the silica sand particles were captured successively in most of the simulations compared to SMT

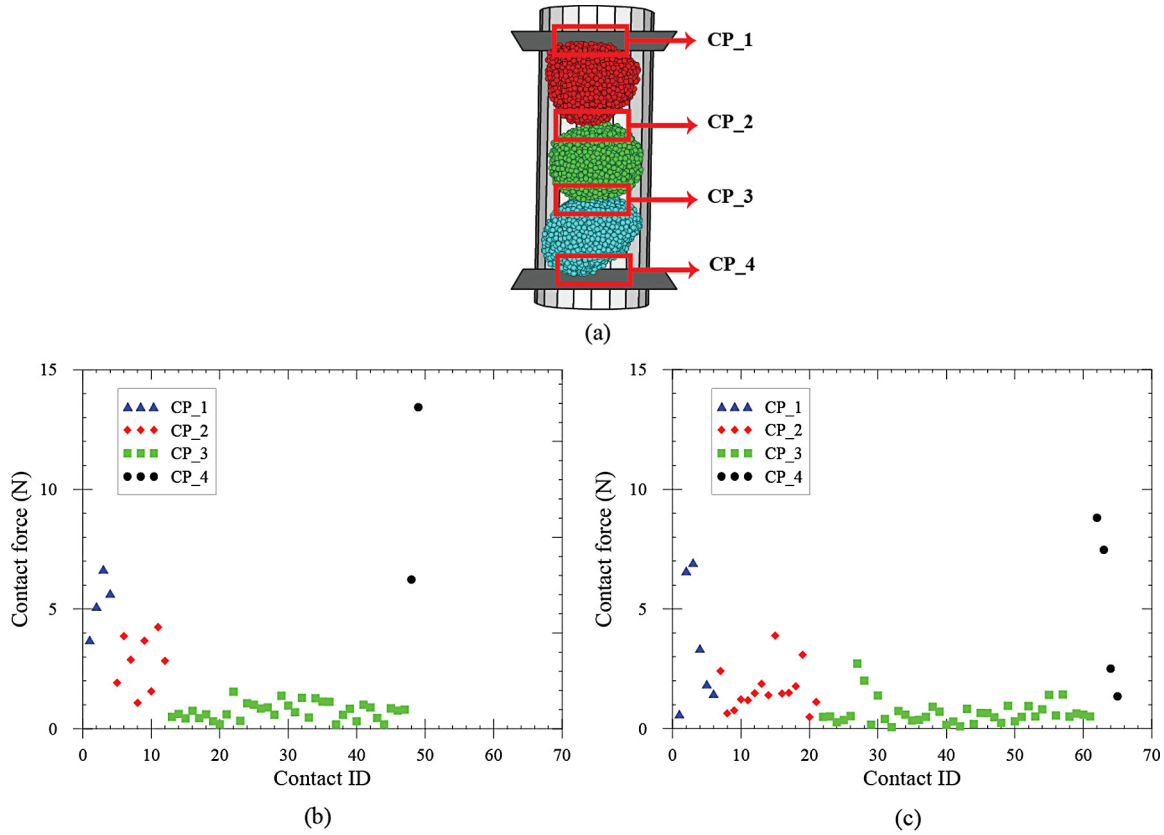

Fig. 4. (Color online.) (a) Description of the analyzed contact points; (b) the number and magnitude of contact forces at CP_1–CP_4 contact points for Test_1a; (c) the number and magnitude of contact forces at CP_1–CP_4 contact points for Test_1d.

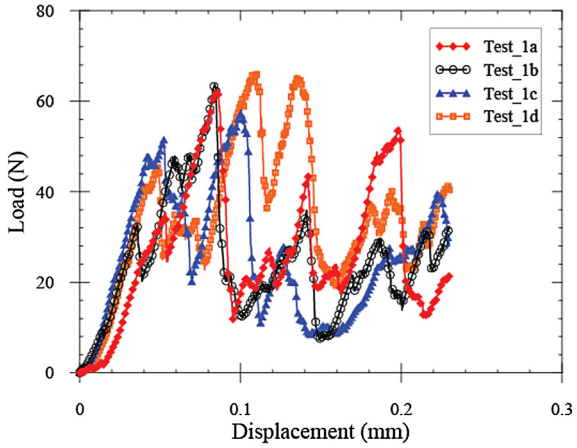

Fig. 5. (Color online.) Load displacement relationship of the first set of DEM simulations.

images. Moreover, the orientations of the particles within the assembly were also reproduced well in the DEM model. Both sets of simulations exhibit a similar initial elastic response under 1D compression loading until the onset of local failures mostly at contact points, which resulted in shifts in the load–displacement curves in DEM simulations. Small load variations before the major particle split fracture were also observed in the experimental results. The influence of size distribution of spherical sub-particles and contact zone interactions became more visible in the fracture mode analysis. In the SMT experiment, the middle sand particle split into fragments after the first major failure, which was followed by the fracture of the top sand particle. On the other hand, the middle or bottom agglomerates exhibited fracture along with some minor failures at contact points in 1D compression simulations. The authors also noticed the fracture of the top agglomerate during

Table 3
Summary of the second set of DEM simulations.

Test	R_{min} (mm)	R_{max}/R_{min}	# of spherical sub-particles				Simulation time (min)
			Agg_1	Agg_2	Agg_3	Total	
Test_2a	2.5×10^{-2}	1	2723	2569	2682	7974	127
Test_2b	2.5×10^{-2}	1.4	1581	1488	1574	4643	62
Test_2c	2.5×10^{-2}	1.8	996	925	999	2920	39
Test_2d	2.5×10^{-2}	2.2	679	633	678	1990	29

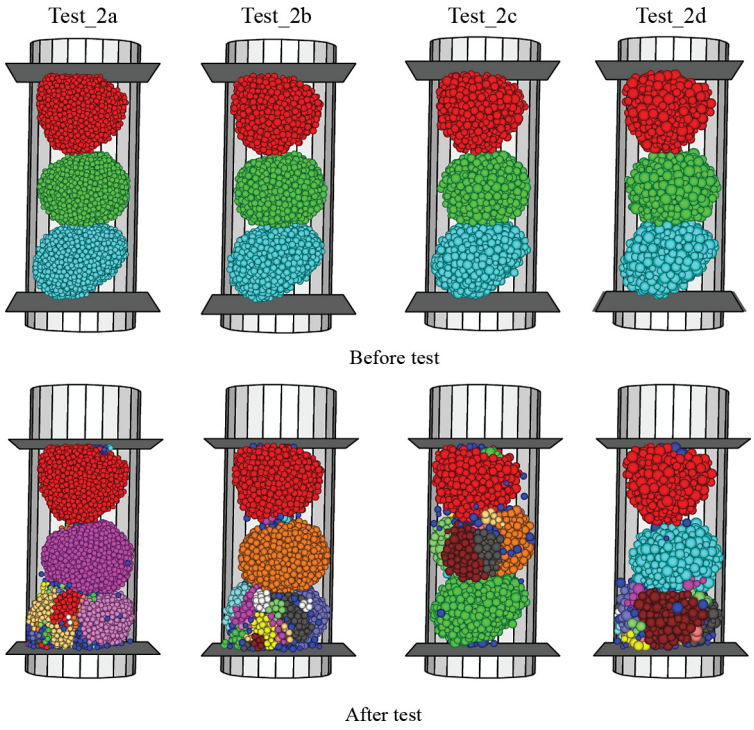

Fig. 6. (Color online.) Axial view of the second set of DEM simulations before and after the 1D compression.

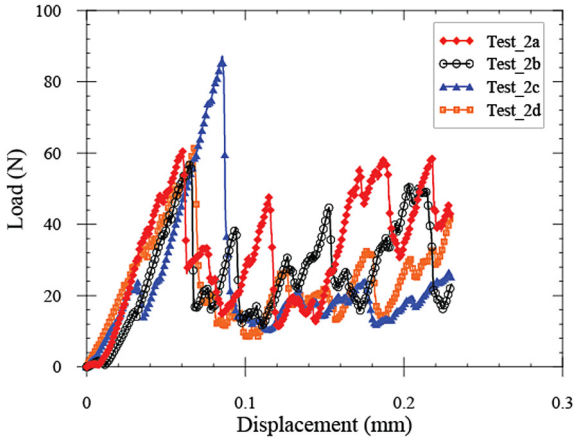

Fig. 7. (Color online.) Load versus displacement relationship of the second set of simulations.

the sensitivity analysis. These DEM simulations clearly demonstrated that contact interactions which are strongly related to spherical sub-particle size considerably influence the fracture behavior of individual agglomerates and overall deformation behavior of the specimen.

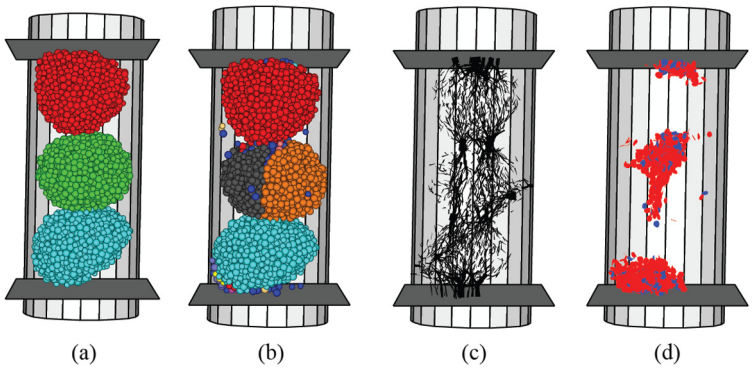

Fig. 8. (Color online.) Axial view of the Test_1c simulation (a) before and (b) after the 1D compression; (c) contact force network; and (d) bond breakages at 0.12 mm displacement.

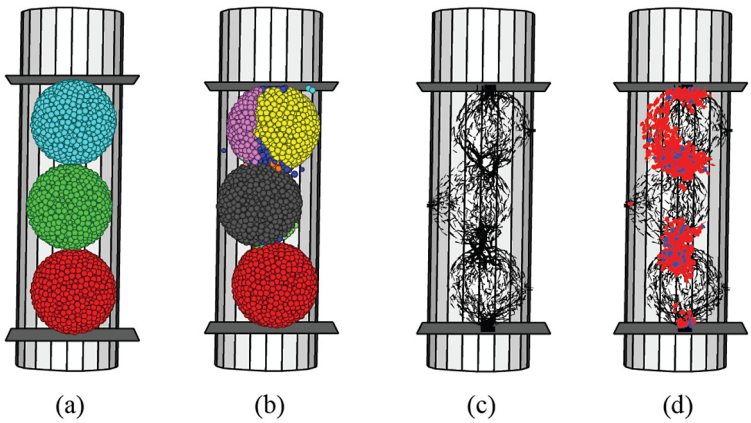

Fig. 9. (Color online.) Axial view of the Test_3 simulation (a) before and (b) after the 1D compression; (c) contact force network; and (d) bond breakages at 0.12 mm displacement.

4.2. Influence of agglomerate shape on fracture behavior

Mapping the 3D physical shape of sand particles into the DEM model provides promising results for future models. Since many studies in the literature adopted agglomerates that have a spherical shape, it is important to identify the differences between agglomerates with spherical shape and 3D physical shape. Therefore, Test_1c simulation was also modeled using spherical agglomerates (Test_3) using the same model parameters and almost same number and size of spherical sub-particles. Axial views of Test_1c and Test 3 simulations before and after 1D compressive loading are depicted in Figs. 8 and 9, which also include the contact force network and the bond breakages within the agglomerates at 0.12 mm displacement. Referring to Figs. 8 and 9, the shapes of the agglomerates change the orientation of particles in the cylindrical mold. The contacts between spherical agglomerates are relatively small compared to agglomerates that closely match the physical shape of sand particles, which significantly influenced the force transmission between particles and the overall response of specimen under 1D compression loading.

The first major fracture occurred at different agglomerates in two simulations (the middle agglomerate in Test_1c) and (the top agglomerate in Test_3), which is attributed to a variation in force transfer and particle orientation. The contact forces are localized at relatively small zones in spherical agglomerates when compared to non-spherical agglomerates as shown in Figs. 8 and 9. Moreover, contact forces are distributed in multiple directions within the spherical agglomerates due to their symmetrical structure. Fig. 8d and Fig. 9d display the distribution and type of bond breakages (micro-cracks) denoted by red and blue hexagons to represent the parallel-bond tensile (normal) and parallel-bond shear failures, respectively. The bond breakages are generally localized at contact points and mostly in the form of tensile failure. The total number of bond breakages in non-spherical agglomerates are 1340 (tensile = 1122, shear = 218) and 1278 (tensile = 1053, shear = 225) in spherical agglomerates. These results indicate that the dominant bond breakage type is same (tensile failure) in both agglomerates; nevertheless, the distribution and evolution of bond breakages are different. The load versus displacement relationships for Test_1c and Test_3 along with experimental measurements are shown in Fig. 10. Similar to previous results, the load versus displacement curves increase initially the load drops at certain stages due to local bond breakages at contact points in both DEM simulations. The major particle fracture occurs at 50 N–60 N load

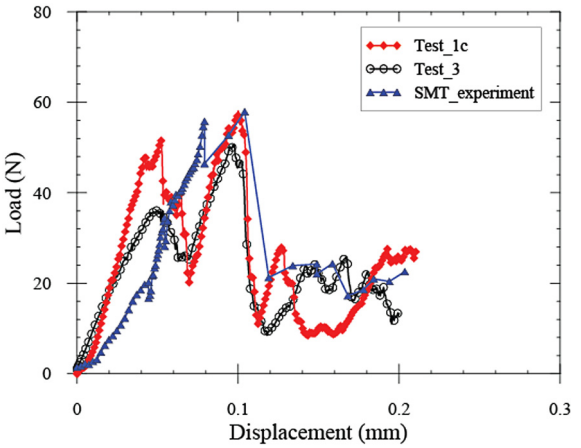

Fig. 10. (Color online.) Load versus displacement relationships for Test_1c and Test_3 DEM simulations and SMT experiment.

range for both DEM simulations and SMT experiment, followed by multiple fluctuations in the load. Since broken fragments continue to fracture after the major particle splitting, particle interactions became more complex as compression progressed.

5. Conclusions

The fracture behavior of sand particles is investigated in DEM using agglomerates that closely match the 3D physical shape of silica sand particles by mapping the 3D particle morphology from the SMT images. The influence of the agglomerate packing and size distribution of spherical sub-particles on fracture behavior were investigated. DEM simulation results show that the size and number of spherical sub-particles are critical in reproducing the physical shape of sand particles accurately. Moreover, it is well known that the surface of contact between the loading platen and the agglomerates greatly affect the load corresponding to failure. On another hand, the numbers of particles change the shape of the agglomerates and therefore the surface of contact between the agglomerates and the loading platen. Agglomerates that closely match the physical shape of sand particles can better reproduce the mode of failure, orientation of particles, and contact configuration when compared to spherical agglomerates.

Acknowledgements

This material is based on work supported by the US National Science Foundation under Grant No. CMMI-1156436. Any opinions, findings, and conclusions or recommendations expressed in this material are those of the authors and do not necessarily reflect the views of the National Science Foundation. The SMT images presented in this paper were collected using the X-ray Operations and Research Beamline Station 13-BMD at Argonne Photon Source (APS), Argonne National Laboratory. We thank Dr. Mark Rivers of APS for help in performing the SMT scans. We also acknowledge the support of GeoSoilEnviroCARS (Sector 13), which is supported by the National Science Foundation, Earth Sciences (EAR-1128799), and the US Department of Energy (DOE), Geosciences (DE-FG02-94ER14466). Use of the Advanced Photon Source, an Office of Science User Facility operated for the DOE Office of Science by Argonne National Laboratory, was supported by DOE under Contract No. DE-AC02-06CH11357. Also, we thank Dr. David Potyondy of Itasca for his valuable comments and assistance.

References

[1] F.N. Altuhafi, M.R. Coop, Changes to particle characteristics associated with the compression of sands, Geotechnique 61 (6) (2011) 459–471, http://dx.doi.org/10.1680/Geot.9.P.114.
[2] M.D. Bolton, Y. Nakata, Y.P. Cheng, Micro- and macro-mechanical behaviour of DEM crushable materials, Geotechnique 58 (6) (2008) 471–480, http://dx.doi.org/10.1680/geot.2008.58.6.471.
[3] I. Cavarretta, C. O'Sullivan, The mechanics of rigid irregular particles subject to uniaxial compression, Geotechnique 62 (8) (2012) 681–692, http://dx.doi.org/10.1680/geot.10.P.102.
[4] S. Lobo-Guerrero, L.E. Vallejo, DEM analysis of crushing around driven piles in granular materials, Geotechnique 55 (8) (2005) 617–623, http://dx.doi.org/10.1680/geot.2005.55.8.617.
[5] G.R. McDowell, O. Harireche, Discrete element modelling of yielding and normal compression of sand, Geotechnique 52 (4) (2002) 299–304, http://dx.doi.org/10.1680/geot.52.4.299.41018.
[6] Y.P. Cheng, Y. Nakata, M.D. Bolton, Discrete element simulation of crushable soil, Geotechnique 53 (7) (2003) 633–641.
[7] Y.P. Cheng, M.D. Bolton, Y. Nakata, Crushing and plastic deformation of soils simulated using DEM, Geotechnique 54 (2) (2004) 131–141, http://dx.doi.org/10.1680/geot.54.2.131.36336.

[8] M.B. Cil, K.A. Alshibli, 3D assessment of fracture of sand particles using discrete element method, Geotech. Lett. 2 (July–September 2012) 161–166.
[9] M.B. Cil, K. Alshibli, Modeling of sand particle fracture using discrete element method and synchrotron micro-tomography images, in: Proceedings of Geo-Congress 2014, GSP 234, Atlanta, GA, USA, ASCE, 2014, pp. 2822–2829.
[10] D.O. Potyondy, P.A. Cundall, A bonded-particle model for rock, Int. J. Rock Mech. Min. Sci. 41 (8) (2004) 1329–1364, http://dx.doi.org/10.1016/j.ijrmms.2004.09.011.